Local Time Variations of High-Energy Plasmaspheric Ion Pitch Angle Distributions

Lois K. Sarno-Smith[1], Michael W. Liemohn[1], Ruth M. Skoug[2], Brian A. Larsen[2], Mark B. Moldwin[1], Roxanne M. Katus[3], John R. Wygant[4]

Corresponding author: Lois K. Sarno-Smith, Department of Climate and Space, University of Michigan, Ann Arbor, Michigan, USA. (loisks@umich.edu)

[1]Department of Climate and Space Sciences and Engineering, University of Michigan, Ann Arbor, Michigan, USA.

[2]Los Alamos National Laboratory, Los Alamos, New Mexico, USA.

[3]Department of Physics, West Virginia University, Morgantown, West Virginia, USA.

[4]Department of Physics and Astronomy, University of Minnesota, Minneapolis, Minnesota, USA.

Abstract.

Recent observations from the Van Allen Probes Helium Oxygen Proton Electron (HOPE) instrument revealed a persistent depletion in the 1-10 eV ion population in the post-midnight sector during quiet times in the $2 < L < 3$ region. This study explores the source of this ion depletion by developing an algorithm to classify 26 months of pitch angle distributions measured by the HOPE instrument. We correct the HOPE low energy fluxes for spacecraft potential using measurements from the Electric Field and Waves (EFW) instrument. A high percentage of low count pitch angle distributions is found in the post-midnight sector coupled with a low percentage of ion distributions peaked perpendicular to the field line. A peak in loss cone distributions in the dusk sector is also observed. These results characterize the nature of the dearth of the near 90^o pitch angle 1-10 eV ion population in the near-Earth post-midnight sector. This study also shows, for the first time, low energy HOPE differential number fluxes corrected for spacecraft potential and 1-10 eV H^+ fluxes at different levels of geomagnetic activity.

1. Introduction

The plasmasphere is a region of cold dense plasma with an average energy of 1 eV that co-rotates with Earth [e.g., *Chappell*, 1972]. The plasmasphere plays a critical role in inner magnetospheric physics, particularly in modulating wave activity [e.g., *Thorne et al.*, 1973; *Kozyra et al.*, 1984; *Bortnik et al.*, 2008]. Changes in plasmaspheric density and composition can lead to changes in the global magnetospheric system. For example, density gradients may change plasmapause location or ion concentrations can disrupt electromagnetic ion cyclotron (EMIC) wave propagation [e.g., *Larsen et al.*, 2007; *Saikin et al.*, 2015].

The high energy tail (1-10 eV) of the inner plasmasphere (L-Shell < 3) ion population exhibits strong local time variation with a minimum in the post-midnight sector [*Lennartsson and Reasoner*, 1978; *Sarno-Smith et al.*, 2015]. Although we show the depletion as a partial density loss, it is also likely a temperature effect where the suprathermal tail of the plasmasphere cools in the post-midnight sector. However, without full density or temperature resolution, we are unable to conclude if the depletion is from temperature, density, or combination of both. A previous study suggested that the 1-10 eV plasmasphere depletion might be linked to ionospheric outflow [*Sarno-Smith et al.*, 2015]. Here, ionospheric outflow refers to the heating of the topside ionosphere and subsequent transport of plasma to the plasmasphere along flux tubes. Topside ionosphere studies have shown post-midnight sector plasma enhancements from downward flow from the plasmasphere, which suggests that this 1-10 eV ion population flows downward along field lines and charge exchanges in the topside ionosphere [*Pavlov and Pavlova*, 2005]. However, the mechanisms leading to the absence of plasma between $2 < L < 3$ remain unresolved.

To further explore the post-midnight depletion of the 1-10 eV ions of the inner plasmasphere, pitch angle distributions of the suprathermal tail (1-10 eV) inner plasmasphere population are analyzed using the Van Allen Probes. Launched in late 2012, the Van Allen Probes are a pair of near equatorial satellites that orbit within geosynchronous orbit [*Mauk et al.*, 2014]. The Helium Oxygen Proton Electron (HOPE) instrument onboard these satellites is a mass spectrometer that measures of H^+, He^+, and O^+ populations of the equatorial inner magnetosphere between 1 eV and 50 keV [*Funsten et al.*, 2014].

The purpose of this study is to determine the cause of the post-midnight sector near-Earth ion depletion and examine the pitch angle distributions of the HOPE H^+ 1-10 eV plasma. In this study, pitch angle distributions are calculated over discrete time windows in the HOPE 1-10 eV ion data to determine when ion fluxes are depleting. A new algorithm is developed to sort pitch angle distributions over a 26 month period. If the depletion is from charge exchange in the top side ionosphere, we expect to see strong field aligned 1-10 eV ion flows across the dayside, particularly at dawn, and a residual equatorially mirroring population that lingers across the night side. For the first time, the results of this study demonstrate that the near 90^o pitch angle 1-10 eV ion population shows a strong depletion in the post-midnight sector while the H^+ ions at pitch angles near 0^o and 180^o remain nearly constant. This suggests a steady but weak outward flow from the ionosphere across the nightside. This behavior suggests that physical processes other than charge exchange and ionospheric influence may be involved in the depletion of the post-midnight sector H^+ 1-10 eV ions. The ion depletion may also be the result of a temperature effect, where the 1-10 eV ions are cooled across the post-midnight sector and thus invisible to HOPE. This new data set thus allows a detailed examination of the diurnal behavior of the inner plasmasphere.

2. Methodology

This study explores the HOPE pitch angle dependence as a function of MLT and L-Shell during quiet times. To do so, 26 months of HOPE H^+ data from February 2013 to April 2015 were sorted by 0.25 L-Shell and 0.5 MLT bins for each energy channel measured by HOPE between 1-10 eV. This time frame encompassed a full precession of the Van Allen Probes satellites. Only times with Kp less than 3 were examined. The polar angle resolution on the HOPE instrument is 18 degrees full width and the azimuthal angle is 4.5 degrees full width half maximum, which allowed for resolution of the loss cone at approximately L = 2, where the loss cone is approximately 16 degrees, but not at L = 3, where the loss cone is approximately 8.4 degrees. HOPE data are routinely binned into 11 pitch angle bins, with centers between 4.5-175.5 degrees. Pitch angle bins are 18 degrees wide, except for 9 degree bins centered at 4.5 and 175.5 degrees. In every spin period of approximately 11 seconds, HOPE differential number flux values were calculated and assigned a pitch angle designation based on the magnetic field direction as measured by the Electric and Magnetic Field Instrument Suite and Integrated Science [*Kletzing et al.*, 2013].

Plasmapause location varies with activity level at time. In particular, the plasmasphere erodes during geomagnetic storms and the plasmapause can be within L < 2 during times of high convection [*Spasojević et al.*, 2003]. However, plasmapause location variability should not significantly affect the results of our statistical study over 2013-2015, which were remarkable years in their absence of storms. In 2013, there are only two storms, March 17, 2013 and June 1, 2013, that are notable and capable of pushing the plasmapause to L < 3. In 2014, there are no significant storms, and in the first part of 2015 (till April), there is only the March 17, 2015 storm. For these dates, we should be concerned about plasmapause location leading to unnaturally low plasma densities between 2 < L < 3. However, three days is statistically insignificant in the context of our larger study of > 600 days. We also have approximately 6 months of dwell time in the post-midnight sector between 2 < L < 3 for our study.

Figure [illegible] shows the 1.5 eV, 3.0 eV, and 5.3 eV H^+ spacecraft potential corrected average differential number fluxes as a function of pitch angle and MLT over 26 months at L = 2 (L-Shell and MLT bins are labelled by the lower bound of the bin). HOPE differential number fluxes were corrected for spacecraft potential by using the Electric Field and Waves instrument (EFW) spacecraft potential measurements [*Wygant et al.*, 2014]. Both the EFW and HOPE measurements were resampled into 1 minute intervals, and the median spacecraft potential in volts for each interval was added to the energy of each of the 1-10 eV energy channels. The 'new' energy channels and fluxes were then logarithmically interpolated to give flux values at the original HOPE energy channels. Here, logarithmically interpolated means the fluxes were appropriately weighted by the location of the nearest energy channels in log space to the spacecraft potential corrected energy. For example, if there is +0.5 V of spacecraft charge, the HOPE 1.2 eV energy channel actually measures 1.7 eV particles. To calculate the 1.8 eV H^+ fluxes, we logarithmically interpolated the fluxes between the spacecraft potential added energy channels of 1.7 eV and 2.0 eV. We kept only energy channels in the 1-10 eV energy range, even after accounting for spacecraft charge.

Although our study encompasses the 1-10 eV H^+ population, Figure 1 highlights three energy channels which reflect the general behavior of the 1-10 eV HOPE energy range. The plot on the left shows the median differential number flux at all MLTs, including a large plasma depletion in the post-midnight sector between $1 < \mathrm{MLT} < 4$ in the each of the energy channels. In the post-midnight sector, there was an absence of particles with pitch angles around 90^o. However, the pitch angles in the loss cone show less depletion than the PA=90^o fluxes in the post-midnight sector, particularly at 3.0 and 5.3 eV. This implies that the ionosphere is still acting as a weak source of low energy plasma to the inner plasmasphere in the post-midnight sector, but it remains unclear what causes the significant equatorially mirroring population depletion in this region. Also, in the 1.5 eV and 3.0 eV energy channels, the fluxes significantly change from a peak in the near PA = 90^o population at MLT=0 to MLT=1.5 to a minimum or near-isotropic distribution in the near PA = 90^o population at MLT=2.5.

The plots in the right column of Figure 1 show the relative variability, or the standard deviation (σ_D) divided by the mean (μ). We have used fraction instead of percent to quantify the uncertainty and variability of the measurements to be consistent with our earlier studies on this subject [*Sarno-Smith et al.*, 2015]. For 1.5 eV and 3.0 eV, the relative variability is higher in the post-midnight sector, especially at pitch angles near 0^o and 180^o. Relative variability is lowest at MLT = 6 to 20 at near PA = 90^o. We expect the post-midnight sector to have more variability for several reasons. For example, the areas of space our bins cover are very large. In the post-midnight sector, some plasma within each bin may not be affected by the mechanisms leading to the depletion of plasma in the post-midnight sector. Thus, there are fluxes with order of magnitude or greater differences contained within each bin, leading to a much higher standard deviation. Interestingly, the relative variability in the post-midnight sector is lowest across all MLTs for the 5.3 eV channel. There are fewer measurements in this energy channel at pitch angles close to 0^o and 180^o, which may contribute to the lower variability. Outside the post-midnight sector, variability is higher at all MLTs compared to the 1.5 and 3.0 eV energy channels. *Sarno-Smith et al.* [2015] also found similar variability differences at different MLTs but showed in Figure 7 that although the post-midnight sector had higher relative variability, the bulk of the post-midnight sector 1-10 eV fluxes were still significantly below (greater than an order of magnitude) the 1-10 eV fluxes outside the post-midnight sector.

Figure 2 shows the spacecraft potential corrected fluxes for the 1-10 eV H^+ population binned by L-Shell and MLT from February 2013 to April 2015. The occurrence of the 0.99 eV fluxes is sparse but approximately uniform across all MLTs at L of 2 to 2.5. By 1.5 eV, the occurrence of the 1.5 eV fluxes extends all L-Shells between 1.5 and 4. The low plasma fluxes in the post-midnight sector are seen in all energies between 1-10 eV, although we only show 0.99 to 3.38 eV here.

Figure 3 shows the 1.5 eV, 3.0 eV, and 5.3 eV H^+ median spacecraft potential corrected average differential number fluxes and the relative variability at PA = 90^o binned by L-Shell and MLT for Kp < 1 and Kp < 3 between February 2013 and April 2015. Activity level does have an impact on the behavior of the 1-10 eV ions, and the difference between the post-midnight sector H^+ differential number fluxes and dayside fluxes is smaller at Kp < 1. Differential number fluxes are higher for the Kp < 1 fluxes, especially for the 1.5 eV and 3.0 eV energy channels within L = 3. The relative variability is highest in the post-midnight sector for both activity level designations. We expect the plasmasphere to be sensitive to geomagnetic activity due to erosion and enhanced convection [*Carpenter*, 1967; *Taylor et al.*, 1970; *Horwitz et al.*, 1990; *Katus et al.*, 2015]. However, the general behavior is similar, and we continue to proceed with the designation of Kp < 3 as a definition for quiet time behavior because the distributions are smoother with the increased number of data points.

To better quantify the depletion of the near PA = 90^o population, the 26 months of HOPE pitch angle distributions were classified by their shape. Pitch angles range from 0 to 180 degrees, where 90^o is a locally mirroring population and 0/180 are field aligned/anti-field aligned particle populations. To ensure a statistically significant number of counts in each bin, the counts of ten consecutive approximately 11 second HOPE measurements, which is approximately 10 spacecraft spins, were summed. However, since the HOPE instrument alternates between measuring ion and electrons, this summing occurred over a 220 second period. The median spacecraft potential over this same period was also used to correct the fluxes for spacecraft potential with the same procedure used in Figures 1 and 2. This time window was chosen to provide sufficient counts while limiting spacecraft motion to no more than 0.125 L-Shells at L < 3. Times where HOPE was in perigee mode, where HOPE measures only energies above 26 eV due to high O^+ densities, were excluded. The pitch angle distributions are determined for each energy channel separately without taking into account the pitch angle distribution classification of other energy channels. This binning resulted in a total of 43,309 pitch angle distributions for spacecraft potential corrected 1.5 eV fluxes, 43,628 pitch angle distributions for 3.0 eV, and 44,927 pitch angle distributions for 5.3 eV over the 26 month period in this study.

To calculate the average of each summed pitch angle distribution, a weighting scheme based on the number of counts in each measurement was used. Over a time window, each pitch angle bin differential flux measurement was assigned a weighting factor corresponding to the number of counts the detector measured. The weighting factor was the number of counts at measurement divided by the total number of counts for each pitch angle bin over the time window.

For inclusion in our study, a pitch angle bin had to have at least 10 total counts across a time window. If a summed pitch angle bin had fewer than 10 counts, it was considered invalid. If a summed pitch angle distribution had six or more invalid pitch angle bins, the entire distribution was labelled as an 'Uncategorized' distribution. However, distributions where all pitch angle bins were considered invalid in a given spin were discarded. Fewer than 1% of the total number of pitch angle distributions fell into this category.

To highlight distribution shapes, each summed pitch angle distribution was normalized by the mean flux value of that pitch angle distribution. The normalized flux summed pitch angle distributions were then sorted by a pitch angle distribution identification algorithm, which was loosely based on the pitch angle distribution sorting algorithm developed for Mars Global Surveyor electron distributions [*Brain et al.*, 2007]. The algorithm presented here was empirically designed to work best for the Van Allen Probes HOPE data set, so modification would be necessary for use with another data set.

Figure 4 shows the categories of pitch angle distributions used for this study and the definitions of each category. Each normalized HOPE pitch angle distribution was classified either as Isotropic, Butterfly, Inverse Butterfly, Source Cone, Loss Cone, One-sided Cone, or Uncategorized. The first sort was for Isotropic distributions. A pitch angle distribution is Isotropic if the second highest and second lowest values of the (approximately) 11 point summed distribution were within 20% of each other (2nd max / 2nd min < 1.2). This method provided more consistent results than using the standard deviation because the HOPE instrument measured fluxes could vary up to 3 orders of magnitude across a single pitch angle distribution. This part of the algorithm was particularly sensitive to changes in the isotropic threshold (2nd max / 2nd min). Lowering the threshold increased the number of partial pitch angle distributions that fell into the Loss Cone designation. Raising the threshold did the opposite. We ultimately chose a threshold that preferentially sorted these borderline distributions into the Loss Cone designation. Using the second highest and lowest values also reduced algorithm sensitivity to extreme fluxes.

The algorithm then reclassified the 11 pitch angle bins into five segments. ‘End1’ is the normalized average of the 4.5 and 18.0 pitch angle bins, ‘Intr1’ is the normalized average of the 36.0 and 54.0 bins, ‘Middle’ is the normalized average of the 72.0, 90.0, and 108.0 bins, ‘Intr2’ is the normalized average of the 126.0 and 144.0 bins, and ‘End2’ is the normalized average of the 162.0 and 175.5 bins. The algorithm sorted the normalized summed pitch angle distributions by the relative peaks and troughs of these five segments.

Then, the algorithm screened for Butterfly distributions, where there are peaks in the intermediate pitch angles and troughs at the ends and in the middle. Butterfly distributions are frequently seen in radiation belt electrons, and it has been proposed that wave particle interactions and magnetopause shadowing are responsible for their formation [*Gannon et al.*, 2007; *Horne et al.*, 2007]. In the inner plasmasphere, Butterfly distributions occur when the plasma is in transition between an equatorially mirroring distribution to/from a field aligned population, with peaks in the intermediate portions of the pitch angle distribution. There are data caveats in the categorization of Butterfly distributions since they required the end points of the pitch angle distributions, and the end points ($0^o/180^o$) are the most unreliable.

The next type of distribution the algorithm looked for was the Inverse Butterfly Distribution, where the flux is lowest at intermediate pitch angles. The Inverse Butterfly is an unusual distribution, where particles are simultaneously being lost and flowing into the specified region of space. This distribution was rare and constituted less than 1% of the total number of pitch angle distributions seen by the HOPE instrument. There are also data caveats in the Inverse Butterfly categorization for the same reasons mentioned previously in the Butterfly distribution classification.

Following Butterfly and Inverse Butterfly Distributions, the algorithm searched for Source Cone distributions, which are peaked at both 0 and 180 degrees. In Source Cone distributions, particles are flowing in or out with pitch angles close to 0 or 180, but the near 90^o population is at a relative minimum. After sorting for Source Cone distributions, the algorithm selected for its counterpart: Loss Cone Distributions, which are peaked at 90^o. Loss Cone distributions occur when the near 90^o pitch angle population is at a relative maximum compared to the fluxes at 0^o and 180^o pitch angles, since the low/high pitch angle particles have already been lost. Loss Cone distributions are common in the inner magnetosphere, particularly for equatorial H^+ [*Comfort and Horwitz*, 1981; *André*, 1986; *Sagawa et al.*, 1987; *Giles et al.*, 1994].

The algorithm then checked for One-sided Cone distributions, peaked at either 0 or 180 degrees. One-sided pitch angle distributions, or asymmetric pitch angle distributions, can occur at times of transition, i.e., crossing a terminator. One-sided pitch angle distributions can also indicate asymmetric field aligned flow due to hemispheric seasonal differences [*Lockwood et al.*, 1985; *Giles et al.*, 1994]. For example, when the northern hemisphere is in summer, this hemisphere will have a larger heated ion concentration than the southern hemisphere. Thus, this seasonal difference between the hemispheres will manifest as increased ion flow from the summer hemisphere into the plasmasphere.

After testing each pitch angle distribution for each of these 'ideal' classifications, the algorithm then sorts the partial pitch angle distributions. In these cases, the pitch angle distributions do not have valid measurements for End1 or End2, for example, but still show an identifiable distribution. A valid partial pitch angle distribution includes Intr1, Middle, and Intr2 but is missing one or both of End1 and End2. For the partial pitch angle distributions, the algorithm first sorted for Source Cones, defined now where Intr1 $>$ Middle and Intr2 $>$ Middle. Then, it looked for Loss Cone, now where Intr1 $<$ Middle and Intr2 $<$ Middle. Lastly, the algorithm screened for One-Sided Cones, defined now as Intr1 $<$ Middle $<$ Intr2 or Intr2 $<$ Middle $<$ Intr1. It is important to note that most of the partial pitch angle distributions were sorted into the 'Loss Cone' distribution. Since visually the partial pitch angle distribution sorts compared well with the full distributions, they were included in this study.

Lastly, if the algorithm was unable to find a match in any of the above categories, the normalized pitch angle distribution was sorted as Uncategorized. At 1.5 eV, Uncategorized pitch angle distributions constituted 11% of the total pitch angle distributions across all MLTs. For 3.0 eV, Uncategorized pitch angle distributions were 16% of the total. At 5.3 eV, Uncategorized pitch angle distributions dominated as 40% of the total pitch angle distributions across all MLTs. As seen in the example of Figure 4 this category comprised mostly severely compromised pitch angle distributions, where there was large variability or too few of points to make a sensible categorization. The Uncategorized distributions generally occurred in the post-midnight sector where counts were too low to be statistically significant (up to 100% of the distributions in the near-Earth post-midnight sector).

Figure 5 shows the number of invalid points in each H^+ sorted pitch angle distribution between February 2013 and October 2015. The number of counts were summed across all MLTs at L=2.0. The number of complete/near complete pitch angle distributions with no/few invalid points is highest for the 1.5 eV energy channel. At the higher energy channels around 5.3 eV, the number of invalid point dominated pitch angle distributions becomes the largest category. In our study, the 1.5-4 eV pitch angle distributions are more reliable and generally more complete than the higher energy pitch angle distributions or the pitch angle distributions below 1.5 eV.

Spacecraft charging is a concern for low energy ion measurements in the magnetosphere. The Van Allen Probes were designed to primarily charge slightly positive. It should be noted that spacecraft potential is a function of total plasma density and temperature; however, this study solely focuses on the 1-10 eV fluxes, so changes in the 1-10 eV fluxes may be independent to spacecraft potential changes. Previous studies found that Van Allen Probes spacecraft potential is about 0.75 V in the 2 < L< 3 region and there are not exceptionally large positive potentials in the post-midnight sector [*Sarno-Smith et al.*, 2015, 2016]. Nonetheless, it is important to remember that this positive potential does add some uncertainty to the aforementioned pitch angle distributions at all MLTs even with spacecraft potential corrected fluxes.

3. Results

The algorithm used in this study successfully sorted the summed pitch angle distributions into the categories described above. Then the sorted pitch angle distributions were binned into hourly MLT bins and results from L = 2 to L = 3 were combined to provide more robust statistics. Although this encompasses a large region of space, during quiet times of $Kp < 3$ this region was most likely within the plasmasphere. Therefore it is reasonable to assume there are no large density gradients between L = 2 to L = 3 and to combine distributions.

Figure 6 shows the pitch angle distribution categorizations for the 1.5, 3.0, and 5.3 eV energy channels between $2 < L < 3$ as a function of MLT. The bar chart on the left depicts the number of total summed pitch angle distributions in the Loss Cone, One-sided Cone, Source Cone, Low Counting Statistics ('Uncat' or 'Uncategorized'), and Other categories. The 'Other' category includes Isotropic, Butterfly, and Inverse Butterfly distributions. As energy increases, the counting statistics are lower and the Uncategorized pitch angle contribution becomes larger across all MLTs. The high Uncategorized distribution percentage is further demonstrated by the bar charts on the right which gave the percentage of the total of each of the main categories.

Looking at the plots on the right side of Figure 6 and in the post-midnight sector, $1 < MLT < 4$, the Uncategorized pitch angle distribution contribution is high at all energies, comprising most of the pitch angle distributions in the 3.0 and 5.3 eV energy range. The results of three low energy channels demonstrate how the post-midnight low energy H^+

depletion becomes more pronounced at higher energies, where the 'Uncategorized' designation dominates. Also notable, the Loss Cone distribution peaks at the dusk terminator (MLT=18) or soon after (MLT = 22) at all energies. In the 1.5 eV pitch angle distributions, the Loss Cone distribution peaks at close to midnight midnight, contributing almost 60% of the total distributions at this MLT. This peak coincides with the increased number of Uncategorized distributions, suggesting that there is an enhanced Loss Cone in the dusk sector/pre-midnight and at midnight that evolves into uncategorized, or depleted, pitch angle distributions in the post-midnight sector. Also notable is that in the 3.0 and 5.3 eV energy channels, the Loss Cone peak in the dusk sector occurs earlier, at MLT = 17 for 3.0 eV and at MLT = 16 for 5.3 eV. This suggests the higher energy particles are depleted first across the dusk sector. The One-Sided distribution has a strong and nearly-uniform presence throughout the dayside. The One-Sided distribution is indicative of strong refilling from the summer hemisphere as solar EUV heated the illuminated ionosphere.

The Source Cone distribution was approximately 5% of the total number of pitch angle distributions between MLT=10-12 and MLT=18-4 in the 1.5 eV and 3.0 eV energy channels. The Source Cone percentage contribution at 5.3 eV is very low across all MLTs. Since the Source Cone populations are indicative of ionospheric outflow, which is usually approximately 1 eV or less, the low percentage of Source Cone distributions at higher energies for all MLTs is expected.

4. Conclusions

The 1-10 eV ion population of the inner plasmasphere has been shown to be depleted in the post-midnight sector and reach a minimum at MLT = 3. In this study, pitch angle distributions of the ion fluxes in the HOPE instrument 1-10 eV energy channels from February 2013 to April 2015 were examined to determine the cause of the 1-10 eV H^+ depletion in the post-midnight sector of the plasmasphere. It was found that the near 90^o pitch angle population was severely depleted in the post-midnight sector compared to the field aligned populations. If these lower 1-10 eV fluxes were from pitch angle diffusion and charge exchange, a weak residual equatorially mirroring population would have been present in the post-midnight sector accompanied by large field aligned flows into the ionosphere.

We also show, for the first time, low energy HOPE differential number fluxes corrected for spacecraft potential using EFW measurements. The flux depletion in the post-midnight sector is still present in the spacecraft potential corrected fluxes. Further, we show that the 1-10 eV plasma depletion in the near-Earth post-midnight sector does exhibit some geomagnetic activity dependence. At Kp < 1, the fluxes are higher than at Kp < 3 between 2 < L < 3, particularly in the 1.5 eV and 3.0 eV energy channels.

A new algorithm was developed to categorize summed pitch angle distributions to better quantify why this loss occurs. A peak in Loss Cone distributions in the pre-midnight sector and strong refilling in the dawn sector were noted in the low energy channels. The Loss Cone peak occurred earlier in the dusk sector for the higher energy particles than the lower energy ones. The post-midnight sector was dominated by Uncategorized distributions at higher energies due to low counting statistics, suggesting plasma depletion occurs before the post-midnight sector due to enhanced dusk and midnight Loss Cone distributions. This result has not been seen before, and it suggests that more than simply charge exchange in the top side ionosphere is responsible for the 1-10 eV lower fluxes.

The pitch angle sorting algorithm will be a useful tool for the magnetospheric community and applied to classify pitch angle distributions at higher energy levels. The algorithm could also classify inner magnetosphere electron pitch angle distributions. For example, one could conduct a study about pitch angle distributions on ring current pitch angle scattering or keV particles at L = 4 during substorm injections [e.g., *Lundin et al.*, 1980; *Smith et al.*, 1996]. Also, the results of this study emphasize that source and loss processes in the inner plasmasphere are more complicated than previously anticipated and may involve more wave heating aspects.

Acknowledgments. The Michigan co-authors would like to thank the University of Michigan Rackham Graduate school, NASA, and the NSF for sponsoring this work under grants NWX11AO60G, NWX144AC02G, AGS-1265651 and AGS-1102863. We would also like to thank Alex Shane and Kristie Llera for their contributions. Work at Los Alamos National Laboratory was performed under the auspices of the U.S. Department of Energy, with support from the NASA Van Allen Probes mission and LA-UR-15-29276. Data used to generate figures for this project came from the Van Allen Probes data center at http://www.rbsp-ect.lanl.gov/data_pub/.

References

André, M. (1986), Electrostatic ion waves generated by ion loss-cone distributions in the magnetosphere, in *Annales Geophysicae, Series A-Upper Atmosphere and Space Sciences*, vol. 4, pp. 241–246.

Bortnik, J., R. M. Thorne, and N. P. Meredith (2008), The unexpected origin of plasmaspheric hiss from discrete chorus emissions, *Nature*, *452*(7183), 62–66.

Brain, D., R. Lillis, D. Mitchell, J. Halekas, and R. Lin (2007), Electron pitch angle distributions as indicators of magnetic field topology near Mars, *Journal of Geophysical Research: Space Physics (1978–2012)*, *112*(A9).

Carpenter, D. L. (1967), Relations between the dawn minimum in the equatorial radius of the plasmapause and Dst, Kp, and local K at Byrd station, *Journal of Geophysical Research*, *72*(11), 2969–2971.

Chappell, C. (1972), Recent satellite measurements of the morphology and dynamics of the plasmasphere, *Reviews of Geophysics*, *10*(4), 951–979.

Comfort, R., and J. Horwitz (1981), Low energy ion pitch angle distributions observed on the dayside at geosynchronous altitudes, *Journal of Geophysical Research: Space Physics (1978–2012)*, *86*(A3), 1621–1627.

Funsten, H., R. Skoug, A. Guthrie, E. MacDonald, J. Baldonado, R. Harper, K. Henderson, K. Kihara, J. Lake, B. Larsen, et al. (2014), Helium, Oxygen, Proton, and Electron (HOPE) mass spectrometer for the Radiation Belt Storm Probes mission, in *The Van Allen Probes Mission*, pp. 423–484, Springer.

Gannon, J., X. Li, and D. Heynderickx (2007), Pitch angle distribution analysis of radiation belt electrons based on combined release and radiation effects satellite medium electrons a data, *Journal of Geophysical Research: Space Physics (1978–2012)*, *112*(A5).

Giles, B., C. Chappell, T. Moore, R. Comfort, and J. Waite (1994), Statistical survey of pitch angle distributions in core (0-50 ev) ions from Dynamics Explorer, 1: Outflow in the auroral zone, polar cap, and cusp, *Journal of Geophysical Research: Space Physics (1978–2012)*, *99*(A9), 17,483–17,501.

Horne, R. B., R. M. Thorne, S. A. Glauert, N. P. Meredith, D. Pokhotelov, and O. Santolík (2007), Electron acceleration in the Van Allen radiation belts by fast magnetosonic waves, *Geophysical Research Letters*, *34*(17).

Horwitz, J., R. Comfort, and C. Chappell (1990), A statistical characterization of plasmasphere density structure and boundary locations, *Journal of Geophysical Research: Space Physics*, *95*(A6), 7937–7947.

Katus, R., D. Gallagher, M. Liemohn, A. Keesee, and L. Sarno-Smith (2015), Statistical storm time examination of MLT-dependent plasmapause location derived from IMAGE EUV, *Journal of Geophysical Research: Space Physics*, *120*(7), 5545–5559.

Kletzing, C., W. Kurth, M. Acuna, R. MacDowall, R. Torbert, T. Averkamp, D. Bodet, S. Bounds, M. Chutter, J. Connerney, et al. (2013), The electric and magnetic field instrument suite and integrated science (EMFISIS) on RBSP, in *The Van Allen Probes Mission*, pp. 127–181, Springer.

Kozyra, J., T. Cravens, A. Nagy, E. Fontheim, and R. Ong (1984), Effects of energetic heavy ions on electromagnetic ion cyclotron wave generation in the plasmapause region, *Journal of Geophysical Research: Space Physics (1978–2012)*, *89*(A4), 2217–2233.

Larsen, B., D. Klumpar, and C. Gurgiolo (2007), Correlation between plasmapause position and solar wind parameters, *Journal of Atmospheric and Solar-Terrestrial Physics*, *69*(3), 334–340.

Lennartsson, W., and D. L. Reasoner (1978), Low-energy plasma observations at synchronous orbit, *Journal of Geophysical Research: Space Physics (1978–2012)*, *83*(A5), 2145–2156.

Lockwood, M., J. Waite, T. Moore, J. Johnson, and C. Chappell (1985), A new source of suprathermal O^+ ions near the dayside polar cap boundary, *Journal of Geophysical Research: Space Physics (1978–2012)*, *90*(A5), 4099–4116.

Lundin, R., L. Lyons, and N. Pissarenko (1980), Observations of the ring current composition at $L \leq 4$, *Geophysical Research Letters*, *7*(6), 425–428.

Mauk, B., N. Fox, S. Kanekal, R. Kessel, D. Sibeck, and A. Ukhorskiy (2014), Science objectives and rationale for the Radiation Belt Storm Probes mission, in *The Van Allen Probes Mission*, pp. 3–27, Springer.

Pavlov, A., and N. Pavlova (2005), Mechanism of the post-midnight winter night-time enhancements in NmF2 over Millstone Hill during 14-17 January 1986, *Journal of atmospheric and solar-terrestrial physics*, *67*(4), 381–395.

Sagawa, E., A. Yau, B. Whalen, and W. Peterson (1987), Pitch angle distributions of low-energy ions in the near-earth magnetosphere, *Journal of Geophysical Research*, *92*(A11), 12–241.

Saikin, A., J.-C. Zhang, R. Allen, C. Smith, L. Kistler, H. Spence, R. Torbert, C. Kletzing, and V. K. Jordanova (2015), The occurrence and wave properties of H^+, He^+, and O^+ band EMIC waves observed by the Van Allen Probes, *Journal of Geophysical Research: Space Physics*.

Sarno-Smith, L. K., M. W. Liemohn, R. M. Katus, R. M. Skoug, B. A. Larsen, M. F. Thomsen, J. R. Wygant, and M. B. Moldwin (2015), Postmidnight depletion of the high-energy tail of the quiet plasmasphere, *Journal of Geophysical Research: Space Physics*, *120*(3), 1646–1660.

Sarno-Smith, L. K., B. A. Larsen, R. M. Skoug, M. W. Liemohn, A. Breneman, J. R. Wygant, and M. F. Thomsen (2016), Spacecraft surface charging within geosynchronous orbit observed by the Van Allen Probes, *Space Weather*.

Smith, A., M. Freeman, and G. Reeves (1996), Post midnight VLF chorus events, a substorm signature observed at the ground near L= 4, *Journal of Geophysical Research: Space Physics (1978–2012)*, *101*(A11), 24,641–24,653.

Spasojević, M., J. Goldstein, D. Carpenter, U. Inan, B. Sandel, M. Moldwin, and B. Reinisch (2003), Global response of the plasmasphere to a geomagnetic disturbance, *Journal of Geophysical Research: Space Physics*, *108*(A9).

Taylor, H., H. Brinton, and A. Deshmukh (1970), Observations of irregular structure in thermal ion distributions in the duskside magnetosphere, *Journal of Geophysical Research*, *75*(13), 2481–2489.

Thorne, R. M., E. J. Smith, R. K. Burton, and R. E. Holzer (1973), Plasmaspheric hiss, *Journal of Geophysical Research*, *78*(10), 1581–1596.

Wygant, J., J. Bonnell, K. Goetz, R. Ergun, F. Mozer, S. Bale, M. Ludlam, P. Turin, P. Harvey, R. Hochmann, et al. (2014), The Electric Field and Waves instruments on the Radiation Belt Storm Probes mission, in *The Van Allen Probes Mission*, pp. 183–220, Springer.

PA_Square.pdf

Figure 1. Median measured proton differential number fluxes (cm^{-2} s^{-1} sr^{-1} keV^{-1}) for 26 months of the HOPE instrument binned by pitch angle and MLT for the 1.5 eV, 3.0 eV, and 5.3 eV energy channels at L = 2. The plots on the right are the relative variability, which is the standard deviation (σ_D) divided by the mean (μ) of each MLT-PA bin at L = 2 for the 1.5 eV, 3.0 eV, and 5.3 eV energy channels.

SCFluxesAll.pdf

Figure 2. Median measured proton differential number fluxes (cm^{-2} s^{-1} sr^{-1} keV^{-1}) for 26 months of combined HOPE instrument data binned by L-Shell and MLT for all of the HOPE energy channels between 0.99 eV and 3.38 eV.

sc_correct.pdf

Figure 3. The plots with the rainbow color table show the median spacecraft potential corrected HOPE differential number fluxes at PA = 90^o using EFW spacecraft potential from February 2013 to April 2015 binned by MLT and L-Shell for the 1.5 eV, 3.0 eV, and 5.3 eV energy channels at Kp < 1 and Kp < 3. The purple scale plots show the relative variability (standard deviation divided by mean) of each L-MLT bin for the 1.5 eV, 3.0 eV, and 5.3 eV energy channels at Kp < 1 and Kp < 3

FlowChart.pdf

Figure 4. Flow chart demonstrating how the HOPE pitch angle distribution sorting algorithm works and some of its sample output. On the categorized plots, the dotted green line shows the second highest and second lowest normalized flux values in the 11 point summed pitch angle distribution. The red line shows the 5 segments defined in the green box that the algorithm used to determine pitch angle distribution shape.

counts2.png

Figure 5. The number of invalid points in each classified H^+ pitch angle distribution from February 2013 to April 2015 for 1.5 eV, 3.0 eV, and 5.3 eV summed across all MLTs at L = 2.0 and then normalized by the maximum number of invalid points at each energy.

barplot_2.5eV.pdf

Figure 6. Bar charts showing the result of the HOPE pitch angle distribution sorting procedure for summed pitch angle distributions in the 1.5, 3.0, and 5.3 eV energy channel bins. These charts show the total summed pitch angle distributions between $2 < L < 3$ in increments of 1 MLT hour. We highlight the four main summed pitch angle distribution categories of Loss Cone, One-Sided Cone, Source Cone, and Uncategorized ('Uncat.'). Other includes the Butterfly, Inverse Butterfly, and Isotropic categories. The plots on the left show the total number of pitch angle distributions contributing to each type of distribution. The plots on the right show the percentage of each type in the specified MLT bin.

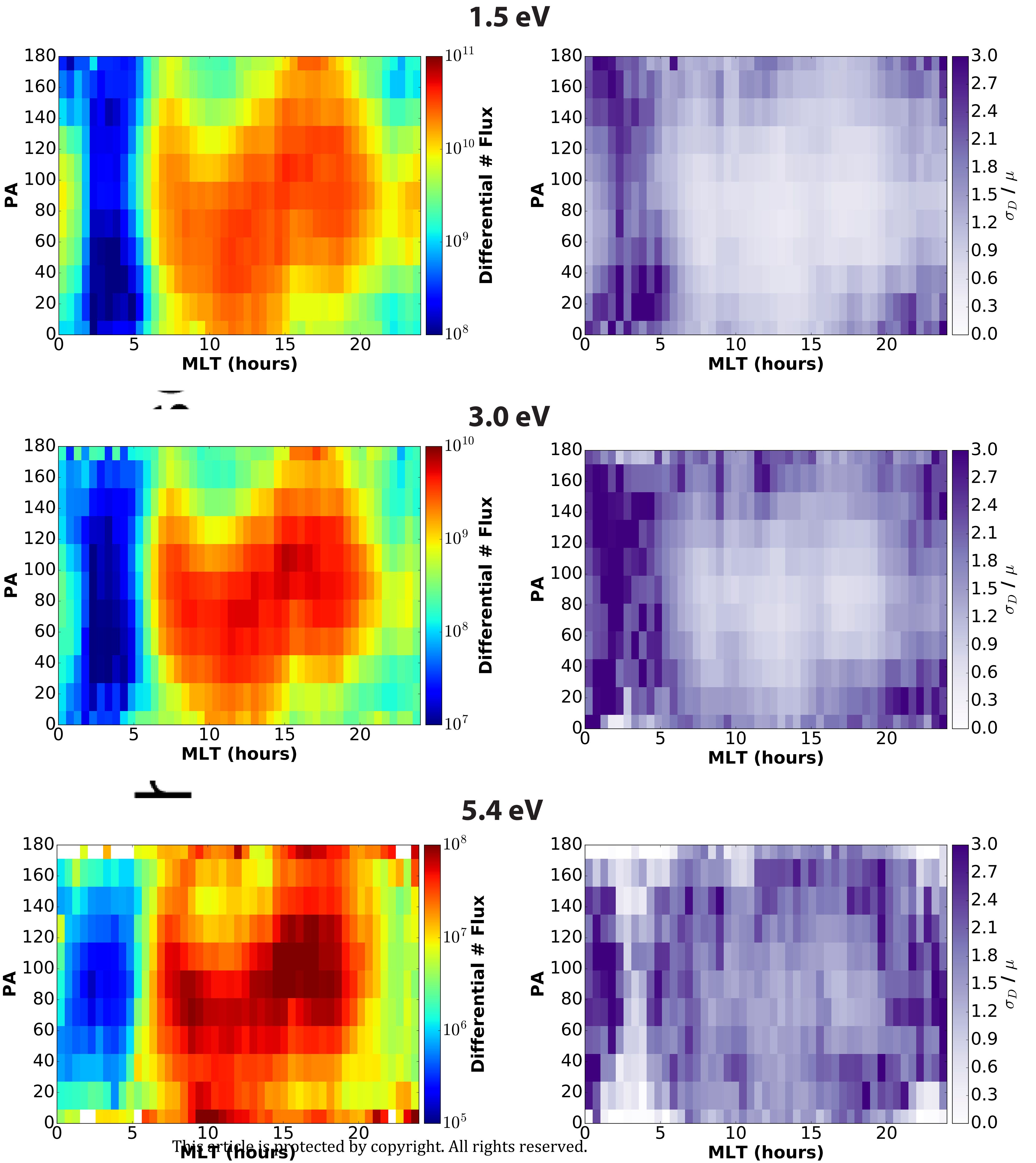

1.5 eV
3.0 eV
5.4 eV
PA
MLT (hours)
Differential # Flux
σ_D / μ

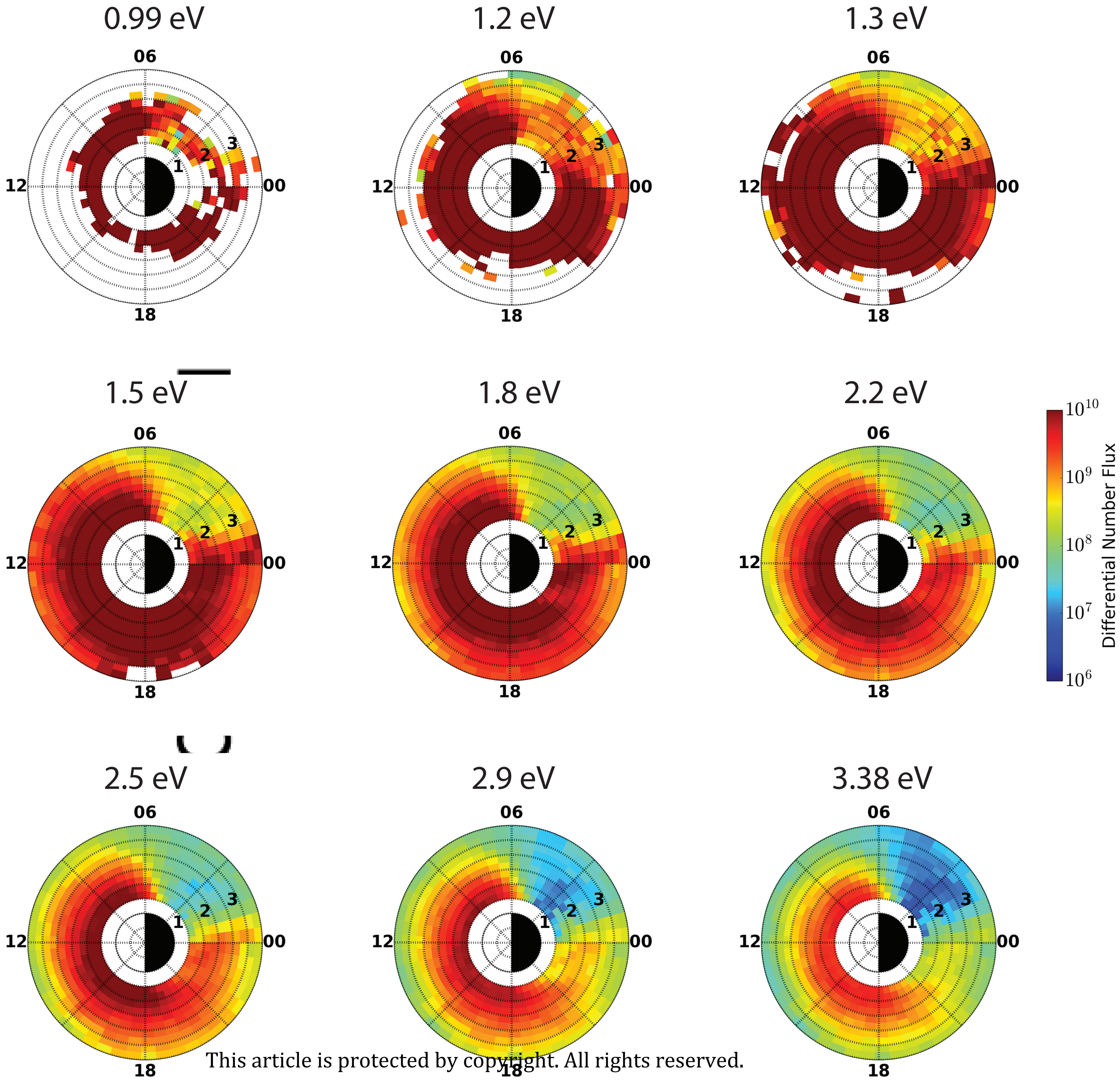
0.99 eV
1.2 eV
1.3 eV
1.5 eV
1.8 eV
2.2 eV
2.5 eV
2.9 eV
3.38 eV
06
12
18
00
1
2
3
Differential Number Flux
10^{10}
10^{9}
10^{8}
10^{7}
10^{6}

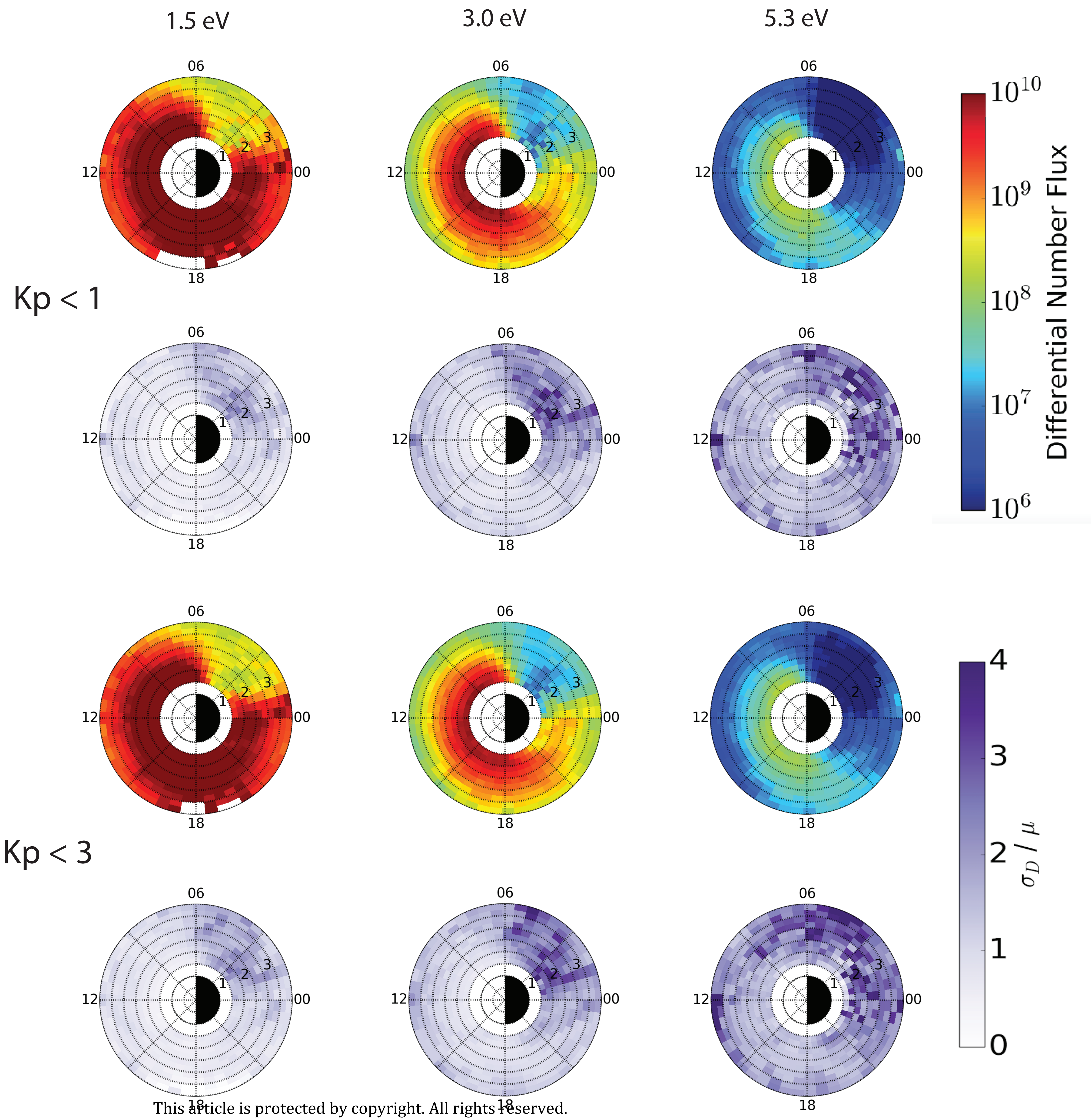
1.5 eV
3.0 eV
5.3 eV
Kp < 1
Kp < 3
06
12
00
18
1
2
3
Differential Number Flux
10^{10}
10^{9}
10^{8}
10^{7}
10^{6}
σ_D / μ
4
3
2
1
0

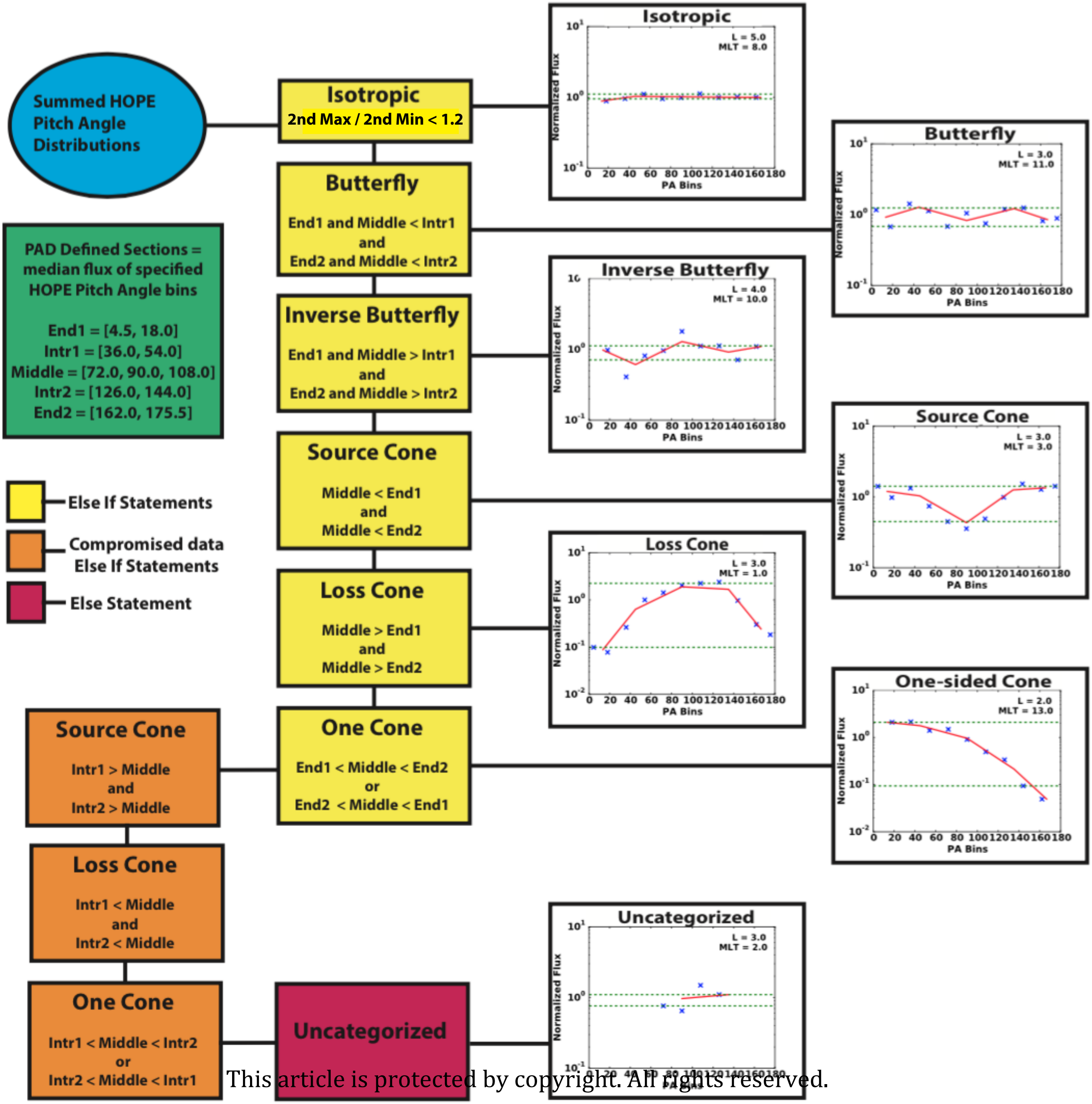
Summed HOPE Pitch Angle Distributions
PAD Defined Sections = median flux of specified HOPE Pitch Angle bins
End1 = [4.5, 18.0]
Intr1 = [36.0, 54.0]
Middle = [72.0, 90.0, 108.0]
Intr2 = [126.0, 144.0]
End2 = [162.0, 175.5]
Else If Statements
Compromised data Else If Statements
Else Statement
Isotropic
2nd Max / 2nd Min < 1.2
Butterfly
End1 and Middle < Intr1 and End2 and Middle < Intr2
Inverse Butterfly
End1 and Middle > Intr1 and End2 and Middle > Intr2
Source Cone
Middle < End1 and Middle < End2
Loss Cone
Middle > End1 and Middle > End2
One Cone
End1 < Middle < End2 or End2 < Middle < End1
Source Cone
Intr1 > Middle and Intr2 > Middle
Loss Cone
Intr1 < Middle and Intr2 < Middle
One Cone
Intr1 < Middle < Intr2 or Intr2 < Middle < Intr1
Uncategorized
Isotropic
L = 5.0
MLT = 8.0
Butterfly
L = 3.0
MLT = 11.0
Inverse Butterfly
L = 4.0
MLT = 10.0
Source Cone
L = 3.0
MLT = 3.0
Loss Cone
L = 3.0
MLT = 1.0
One-sided Cone
L = 2.0
MLT = 13.0
Uncategorized
L = 3.0
MLT = 2.0
Normalized Flux
PA Bins

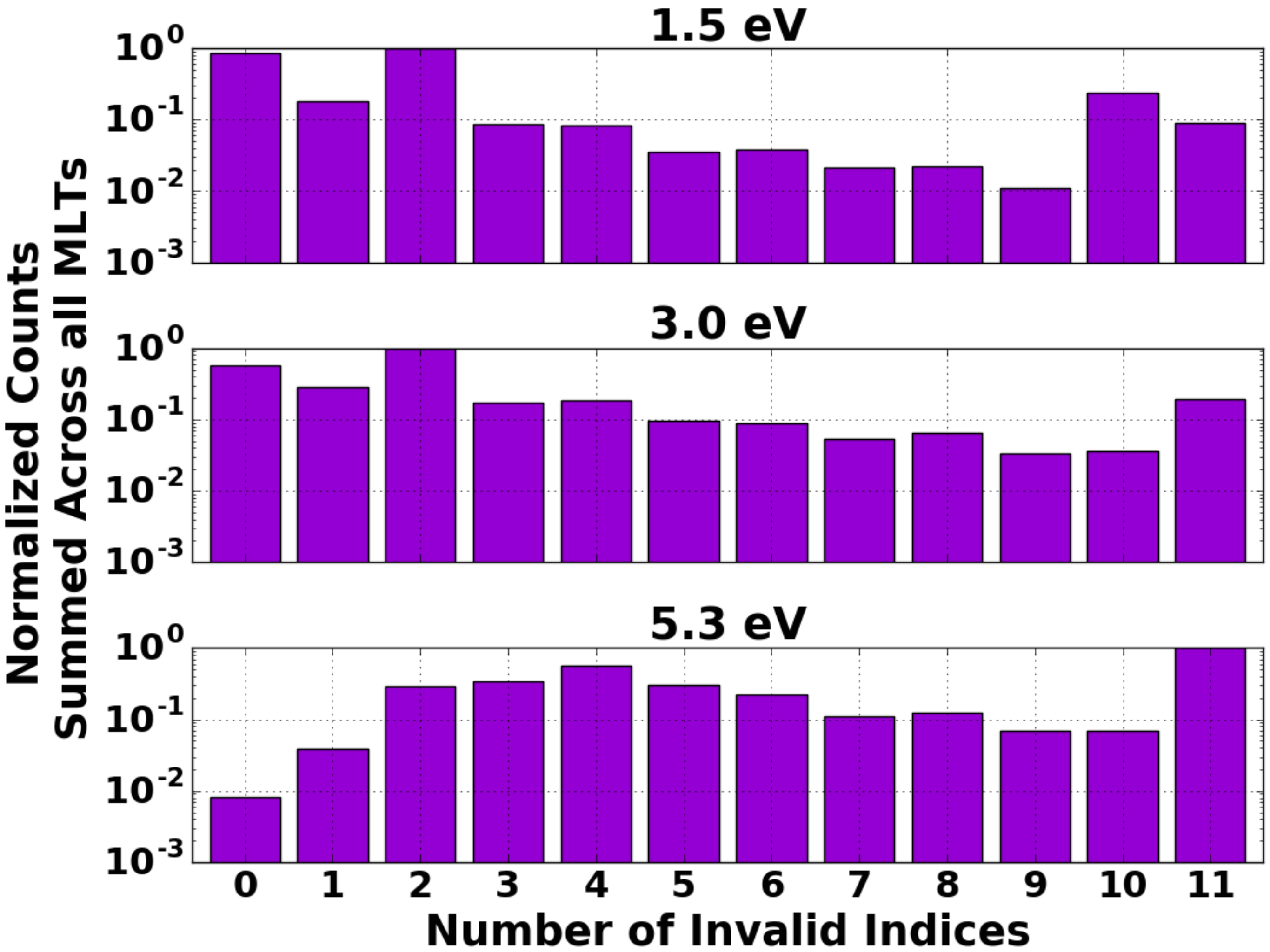

2015JA022301-f05-z-.png

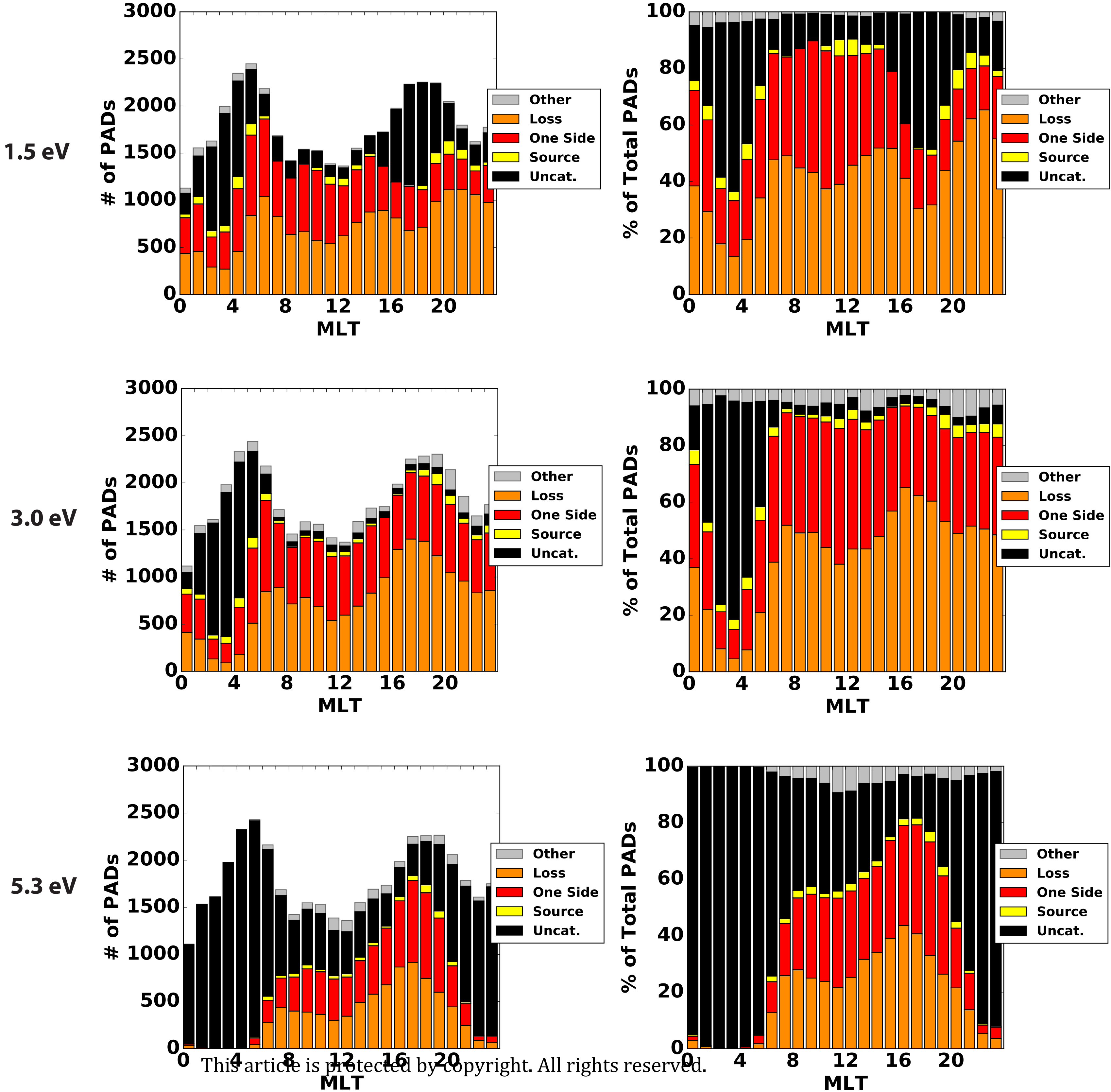
1.5 eV
3.0 eV
5.3 eV
# of PADs
% of Total PADs
MLT
Other
Loss
One Side
Source
Uncat.